Supporting Information

DFT Study of Oxygen Reduction Reaction on Os/Pt Core-Shell Catalysts Validated by Electrochemical Experiment

Ho-Cheng Tsai,[†] Yu-Chi Hsie,[‡,§] Ted H. Yu, [†,‖] Yi-Juei Lee,[§] Yue-Han Wu,[§] Boris V. Merinov,[,†] Pu-Wei Wu,[§] San-Yuan Chen,[§] Radoslav R. Adzic,[‡] and William A. Goddard, III[*,†]*

[†]Materials and Process Simulation Center (M/C 139-74), California Institute of Technology, 1200 East California Boulevard., Pasadena, California 91125, USA

[‡]Chemistry Department, Brookhaven National Laboratory, Upton, NY 11973, USA

[§]Department of Materials Science and Engineering, National Chiao Tung University, Hsin-Chu 300, Taiwan, ROC

[‖]Department of Chemical Engineering, California State University, Long Beach, CA 90840, USA

Corresponding Author

*E-mail: merinov@caltech.edu (B.V. M.)

*E-mail: wag@wag.caltech.edu (W.A. G.)

Figure S1 shows the reaction energy barriers for the OOH formation reaction and H_2O formation reaction in solvated phase. The values are from Table S5. The OOH formation barrier increases vs. an increasing number of Pt deposited layers, while the H_2O formation barrier decreases. The two lines intersect at about 0.22 eV, which approximately corresponds to 2 ML deposited Pt. The RDS is a compromise between stage I and stage III. The best activity is observed for ~2 layers of Pt deposition.

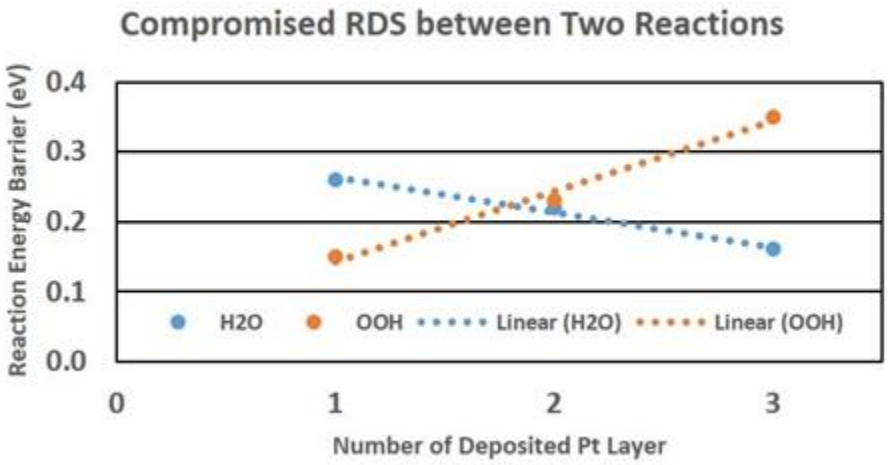

Figure S1. Reaction energy barriers for the OOH formation and H_2O formation reactions vs. a number of deposited Pt layers in solution.

We have analyzed the thermodynamic effect of the electrode potential by examining the Eley-Rideal mechanism. For this, we applied the approach developed by Norskøv et al.[1] In this approach, the reaction energy barriers are assumed to be equal at least to the energy differences of the corresponding endothermic reactions, whereas the exothermic reactions are considered as spontaneous and barrierless.

Since O_2 is not well described by DFT PBE,[2] we set the energy of the reaction $H_{2(g)}+1/2O_{2(g)} \rightarrow H_2O_{(g)}$ to the experimental value of the Gibbs free energy, –2.46 eV.

Therefore, the O_2 energy could be determined by calculating the H_2 and H_2O energies as reference energies. The binding energies of the ORR species in solution (Table S3) were applied for each ORR step of the O_2-diss-hydr and H-OOH-diss mechanisms. Three potentials, 0.00, 0.80 and 1.23 V, were applied in our calculations. The ORR potential energy surfaces for the Eley-Rideal reactions are shown for the O_2-diss-hydr and H-OOH-diss mechanisms in Figures S2 and S3, respectively.

The ORR pathways obtained for the Os, Pt, and Pt/Os surfaces using the Eley-Rideal mechanism are consistent with those resulted from the Langmuir–Hinshelwood mechanism. On the Os surface, the O_2-diss-hydr mechanism is preferable, whereas on the Pt and Pt/Os surfaces, the H-OOH-diss mechanism dominates. At potential lower than 0.80 V, the ORR is almost barrierless for the Pt/Os catalysts with a slightly higher barrier for pure Pt (0.17 eV at 0.80 V). At 1.23 V, the RDS for Pt_{1ML}/Os is the H_2O formation reaction with a barrier of 0.45 eV, while for Pt_{2ML}/Os, Pt_{3ML}/Os, and Pt, the RDS is the OOH formation reaction with a barrier of 0.23 eV, 0.42 and 0.60 eV, respectively. The RDS is again a compromise between the H_2O formation and OOH-formation reactions and Pt_{2ML}/Os is the best among the catalysts considered here.

Figure S2a shows the O_2 reduction via the O_2 dissociation ($O_2 \rightarrow 2O$) and O-hydration ($O+H_2O \rightarrow 2OH$) on Os slab at the three different potentials. The energy difference between the first and last steps at 1.23 V is the H_2O binding energy, since we have set the energy of the reaction $H_{2(g)}+1/2O_{2(g)} \rightarrow H_2O_{(g)}$ to –2.46 eV. We find that the potential-independent O-hydration reaction (0.27 eV) determines the ORR rate at 0 V, while the H_2O formation reaction is the RDS at higher potentials (0.37 eV at 0.80 V and 0.80 eV at 1.23 V).

If we consider the O_2-diss-hydr mechanism on the Pt and Pt/Os surfaces, the O-hydration reaction is the RDS almost for all catalysts (0.65 eV for Pt, 0.31 eV for Pt_{2ML}/Os, and 0.48 eV for Pt_{3ML}/Os), except for Pt_{1ML}/Os, where the O-hydration reaction is practically barrierless and the more sluggish H_2O formation reaction retards the ORR (Figure S2b-e and Table S5). The high barrier for the O-hydration reaction makes the ORR run via the OOH formation, H-OOH dissociation and H_2O formation steps (Figures S3). For Os, the potential-dependent OOH formation reaction has a higher barrier than the H_2O formation reaction. Thus, the O_2-diss-hydr mechanism is more relevant for the ORR on the Os surface.

On the pure Pt surface, the OOH formation reaction, which is the RDS, has a lower barrier than the O-hydration reaction and, therefore, the H-OOH-diss mechanism is preferable on the Pt surface.

On the Pt/Os surfaces, the ORR are almost barrierless at 0 V and 0.80 V. More important is the barrier at a higher potential, because the activation region of the ORR polarization curves begins from ~ 1.00 V vs. RHE (see the ORR curves in section 3.5 Experimental results). At 1.23 V, a compromise between the H_2O and OOH formation reactions determines the ORR rate (similar to Figure S1). The barrier for the H_2O formation reaction decreases with the increasing number of the Pt layers deposited, 0.45, 0.12 and 0.09 eV for Pt_{1ML}/Os, Pt_{2ML}/Os and Pt_{3ML}/Os, respectively. On the other hand, the barrier for the OOH formation reaction generally increases with the increasing number of the deposited Pt layers, 0.26, 0.23 and 0.42 eV for Pt_{1ML}/Os, Pt_{2ML}/Os and Pt_{3ML}/Os, respectively. The best catalyst is, therefore, Pt_{2ML}/Os. This conclusion is consistent with our result for the Langmuir–Hinshelwood mechanism.

In summary, we can say that the results obtained for the Eley-Rideal mechanism agree with those obtained for the Langmuir–Hinshelwood mechanism and do not affect our conclusions.

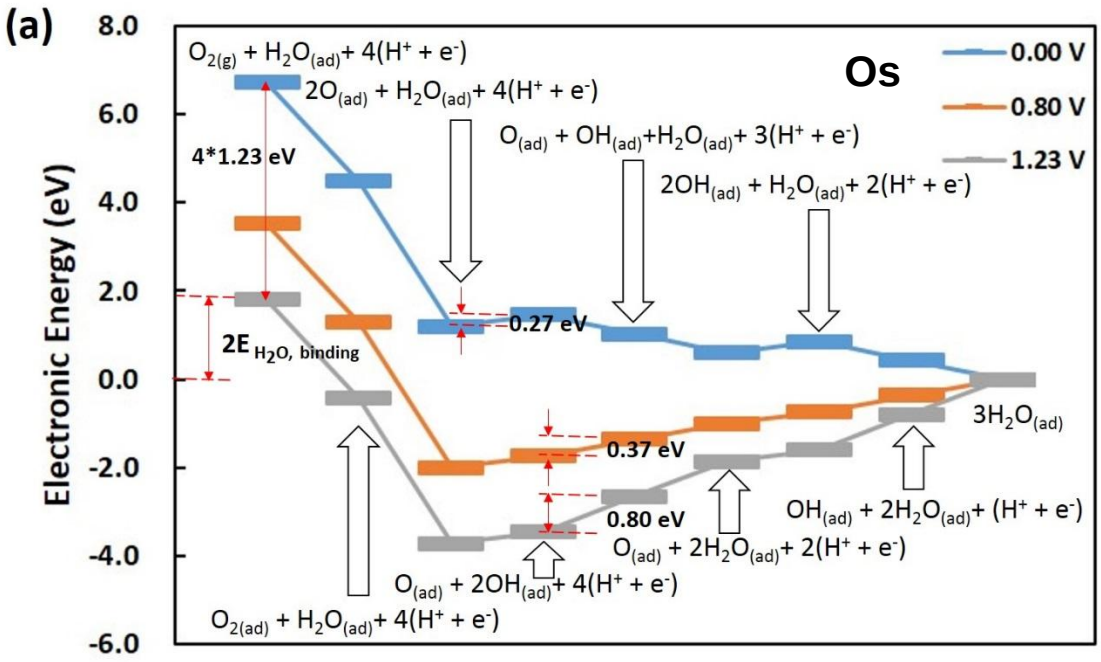

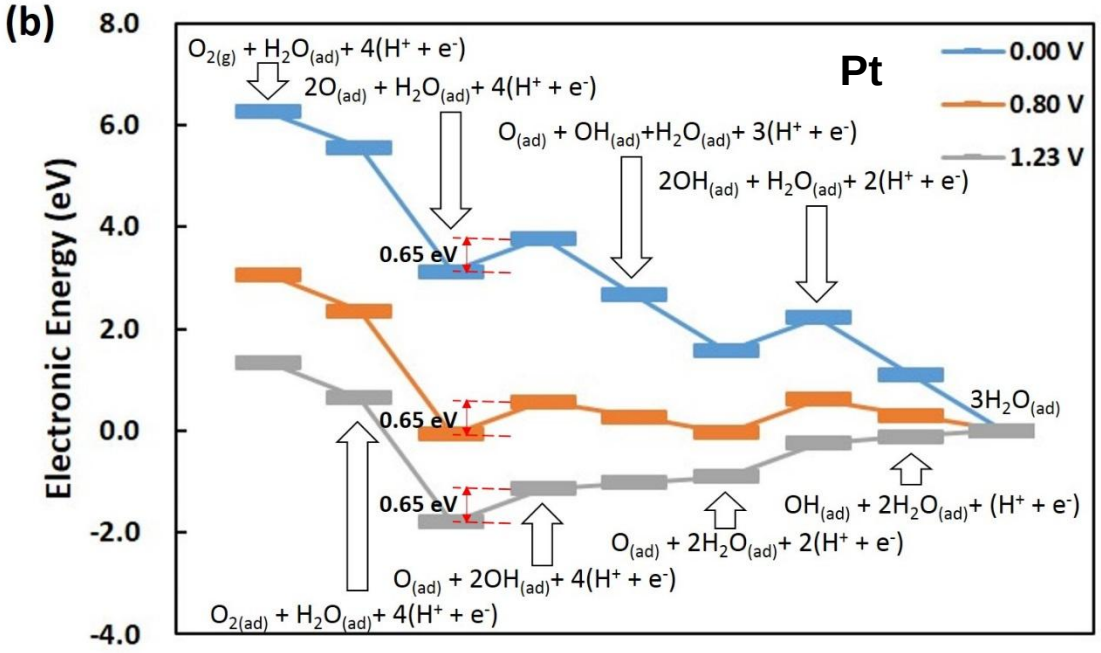
(b)
Pt
0.00 V
0.80 V
1.23 V
Electronic Energy (eV)
8.0
6.0
4.0
2.0
0.0
-2.0
-4.0
O2(g) + H2O(ad)+ 4(H+ + e-)
2O(ad) + H2O(ad)+ 4(H+ + e-)
O(ad) + OH(ad)+H2O(ad)+ 3(H+ + e-)
2OH(ad) + H2O(ad)+ 2(H+ + e-)
0.65 eV
0.65 eV
0.65 eV
3H2O(ad)
OH(ad) + 2H2O(ad)+ (H+ + e-)
O(ad) + 2H2O(ad)+ 2(H+ + e-)
O(ad) + 2OH(ad)+ 4(H+ + e-)
O2(ad) + H2O(ad)+ 4(H+ + e-)

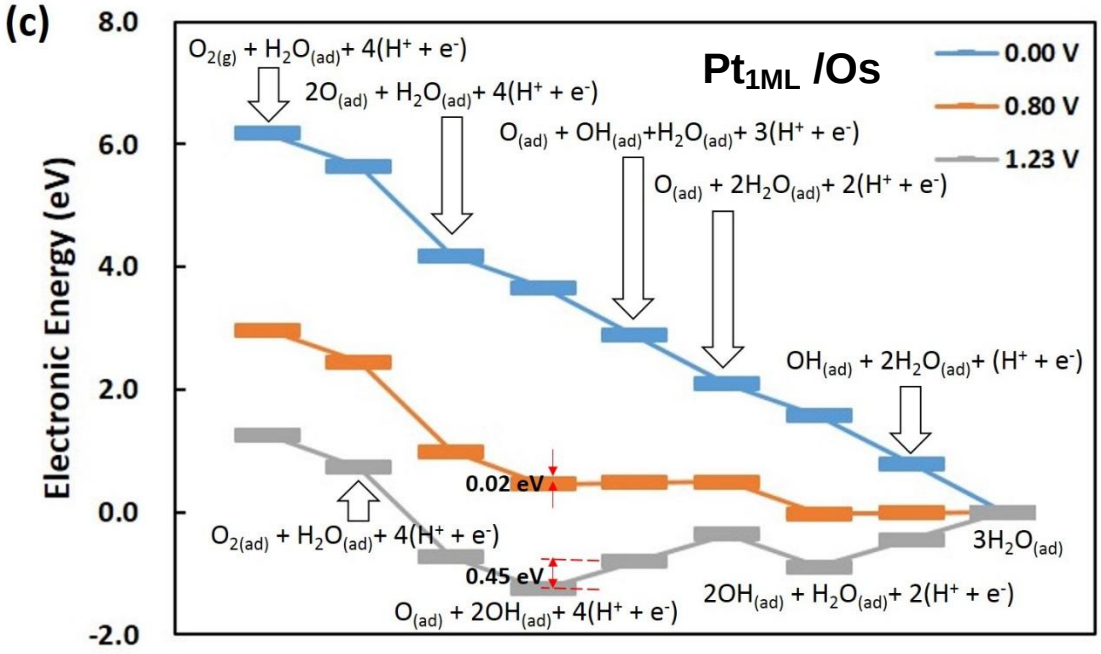
(c)
Pt1ML /Os
0.00 V
0.80 V
1.23 V
Electronic Energy (eV)
8.0
6.0
4.0
2.0
0.0
-2.0
O2(g) + H2O(ad)+ 4(H+ + e-)
2O(ad) + H2O(ad)+ 4(H+ + e-)
O(ad) + OH(ad)+H2O(ad)+ 3(H+ + e-)
O(ad) + 2H2O(ad)+ 2(H+ + e-)
OH(ad) + 2H2O(ad)+ (H+ + e-)
0.02 eV
O2(ad) + H2O(ad)+ 4(H+ + e-)
3H2O(ad)
0.45 eV
2OH(ad) + H2O(ad)+ 2(H+ + e-)
O(ad) + 2OH(ad)+ 4(H+ + e-)

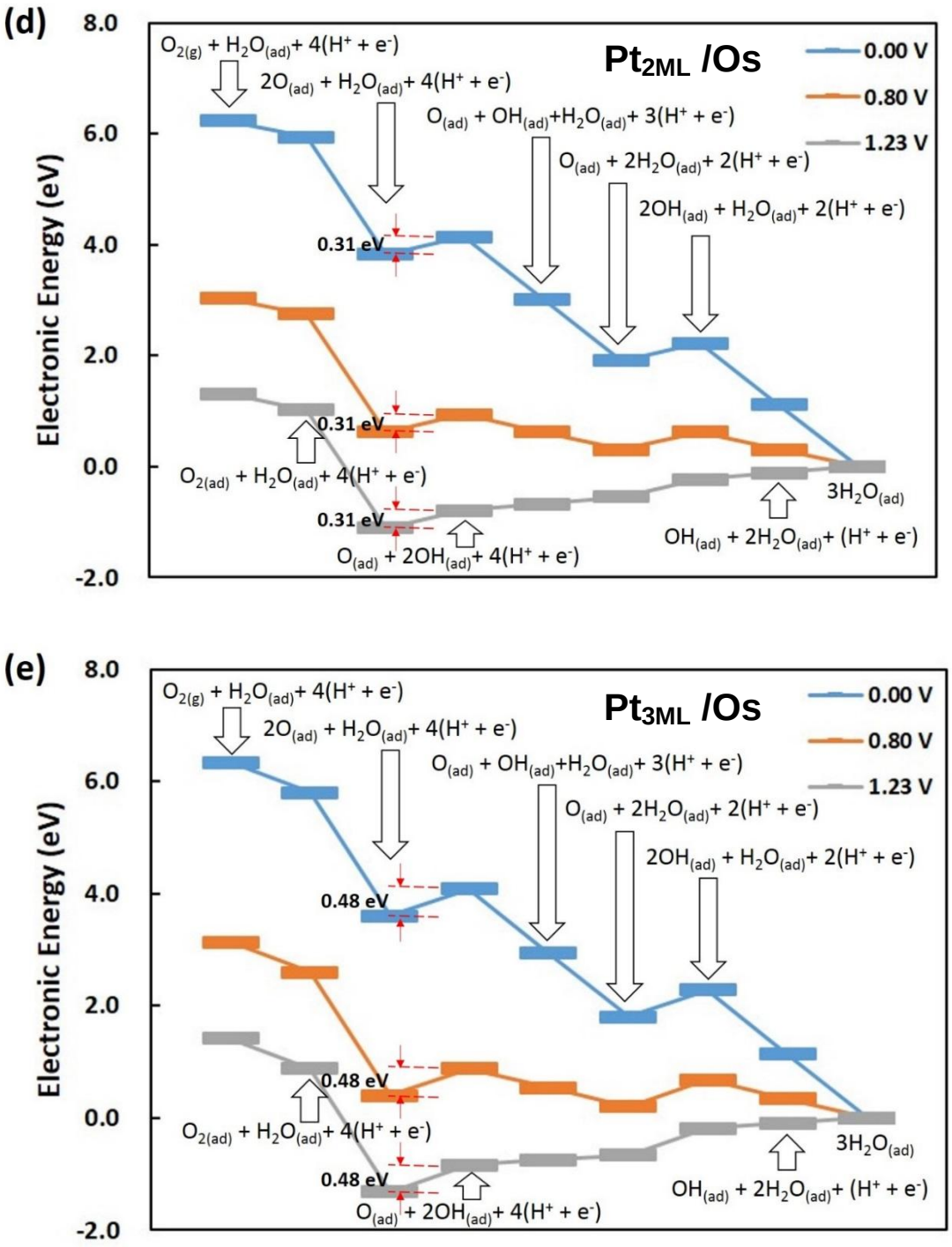

Figure S2. Potential energy surfaces for the O_2-diss-hydr mechanism for Os (a), Pt (b), Pt_{1ML}/Os (c), Pt_{2ML}/Os (d), and Pt_{3ML}/Os (e) in solution.

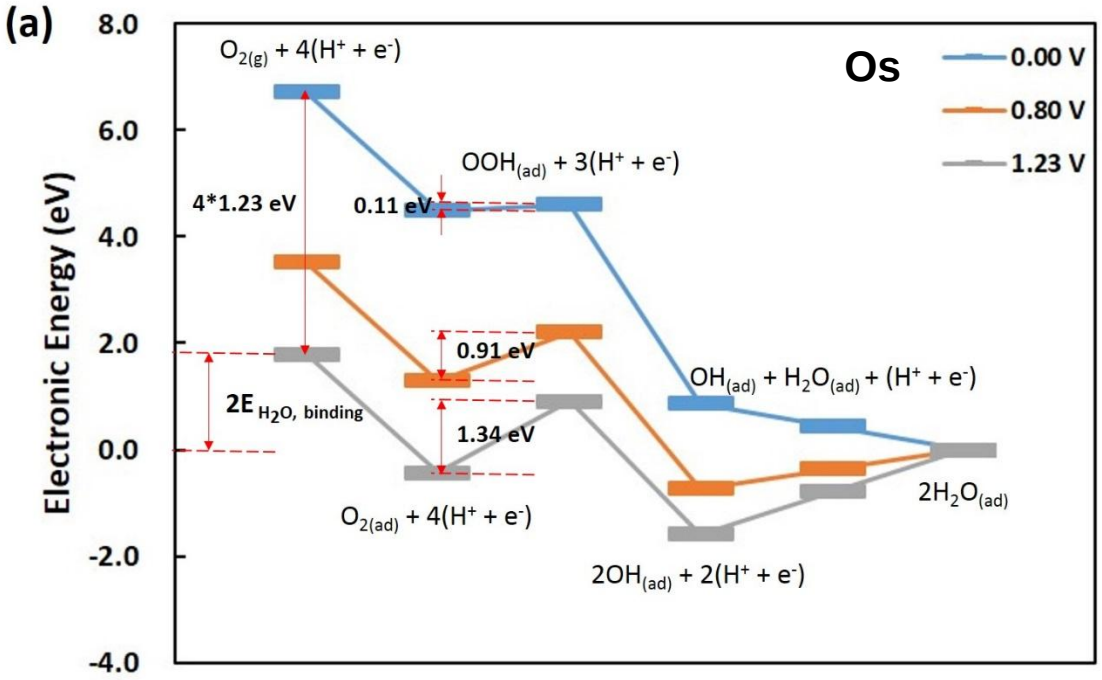
(a)
Os
0.00 V
0.80 V
1.23 V
Electronic Energy (eV)
8.0
6.0
4.0
2.0
0.0
-2.0
-4.0
O2(g) + 4(H+ + e-)
OOH(ad) + 3(H+ + e-)
OH(ad) + H2O(ad) + (H+ + e-)
2H2O(ad)
O2(ad) + 4(H+ + e-)
2OH(ad) + 2(H+ + e-)
4*1.23 eV
0.11 eV
0.91 eV
1.34 eV
2E H2O, binding

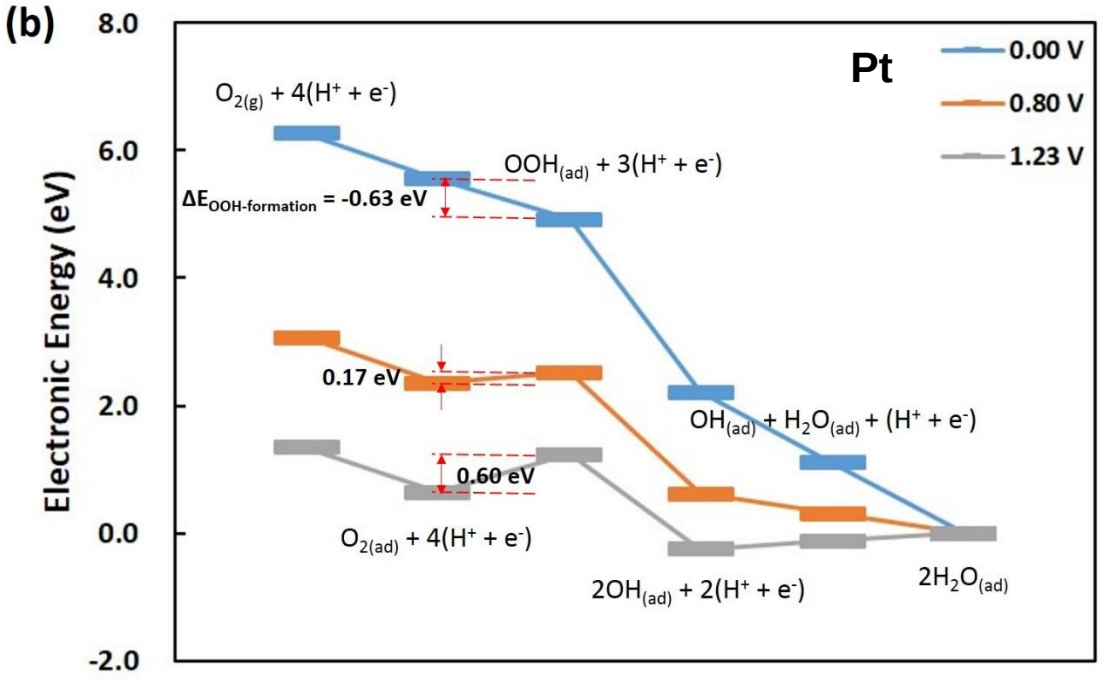
(b)
Pt
0.00 V
0.80 V
1.23 V
Electronic Energy (eV)
8.0
6.0
4.0
2.0
0.0
-2.0
O2(g) + 4(H+ + e-)
OOH(ad) + 3(H+ + e-)
OH(ad) + H2O(ad) + (H+ + e-)
2H2O(ad)
O2(ad) + 4(H+ + e-)
2OH(ad) + 2(H+ + e-)
ΔEOOH-formation = -0.63 eV
0.17 eV
0.60 eV

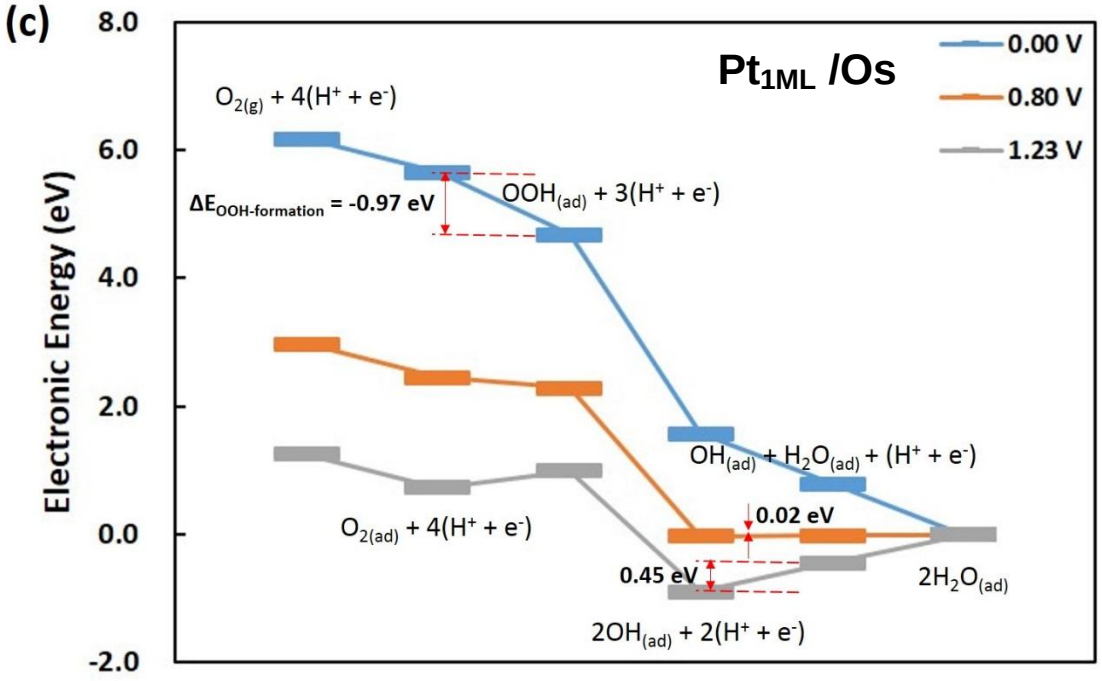
(c)
Pt1ML /Os
0.00 V
0.80 V
1.23 V
Electronic Energy (eV)
8.0
6.0
4.0
2.0
0.0
-2.0
O2(g) + 4(H+ + e-)
ΔEOOH-formation = -0.97 eV
OOH(ad) + 3(H+ + e-)
OH(ad) + H2O(ad) + (H+ + e-)
0.02 eV
O2(ad) + 4(H+ + e-)
0.45 eV
2H2O(ad)
2OH(ad) + 2(H+ + e-)

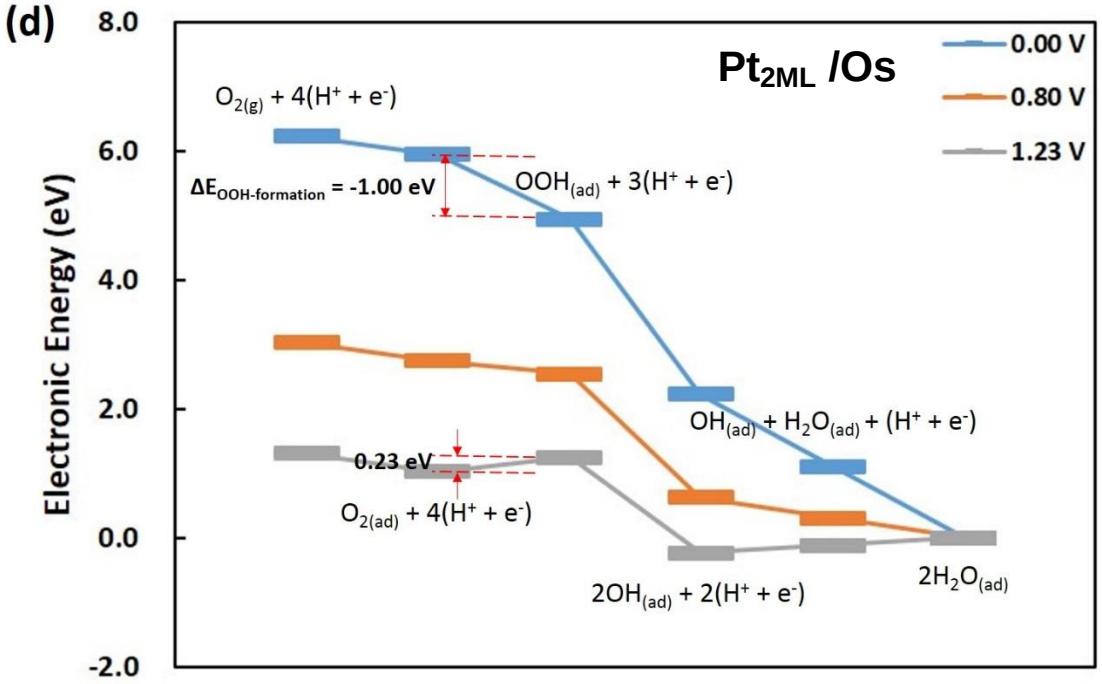
(d)
Pt2ML /Os
0.00 V
0.80 V
1.23 V
Electronic Energy (eV)
8.0
6.0
4.0
2.0
0.0
-2.0
O2(g) + 4(H+ + e-)
ΔEOOH-formation = -1.00 eV
OOH(ad) + 3(H+ + e-)
OH(ad) + H2O(ad) + (H+ + e-)
0.23 eV
O2(ad) + 4(H+ + e-)
2OH(ad) + 2(H+ + e-)
2H2O(ad)

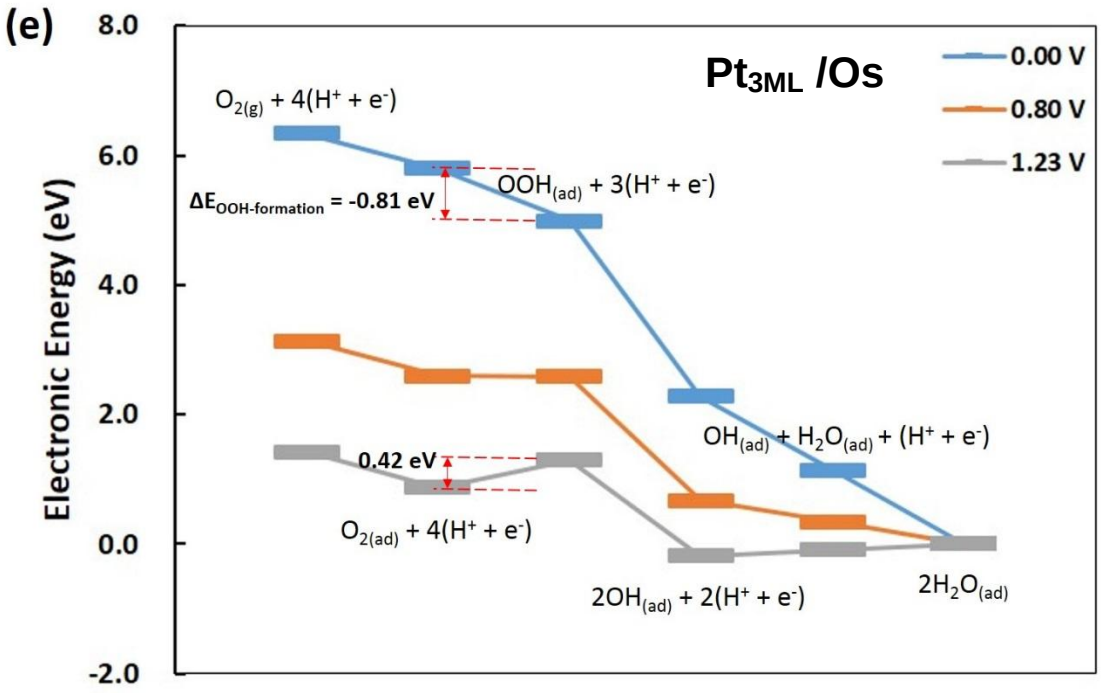

Figure S3. Potential energy surfaces for the H-OOH-diss mechanism for Os (a), Pt (b), Pt_{1ML}/Os (c), Pt_{2ML}/Os (d), and Pt_{3ML}/Os (e) in solution.

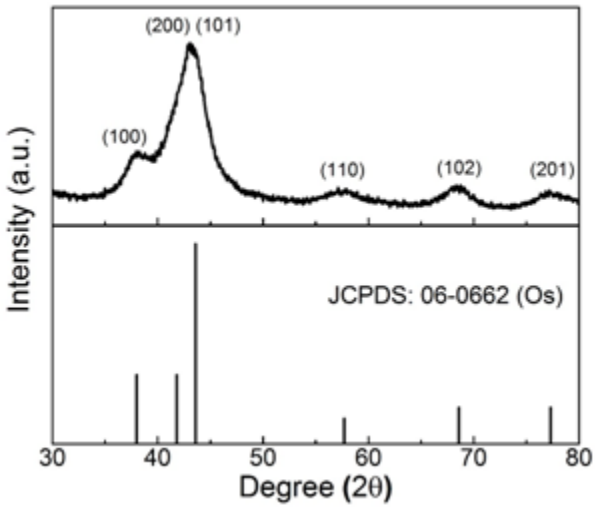

Figure S4. X-ray diffraction patterns of Os/C and hcp Os (JCPDS: 006-0662).

Figure S5 shows the CV curves for Os/C, Pt_{1ML}/Os/C, Pt_{2ML}/Os/C for ESCA determination. It is very clear that in this magnifying figure, Os/C and Pt_{1ML}/Os/C have extra current density than Pt_{2ML}/Os/C in the double layer region (0.3~0.6V vs. NHE) because of the oxidation of exposed Os atoms.

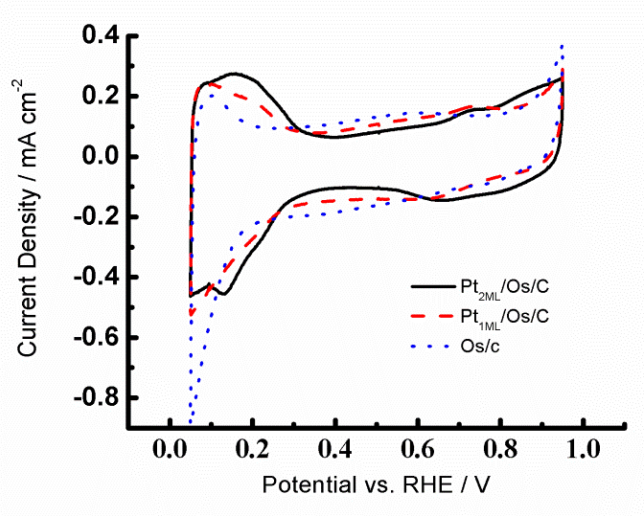

Figure S5. The CV curves for ECSA determination for Os/C, Pt_{1ML}/Os/C and Pt_{2ML}/Os/C, respectively. The electrolyte was deaerated 0.1 M aqueous $HClO_4$.

Figure S6 shows correlation between the experimental half wave potential and theoretically calculated OH binding energy. Previous experimental studies[3] indicate good agreement with a theoretical study in which the maximum activity corresponds to the surface that could bind OH by ~0.1 eV weaker than Pt.[4,5] Our result indicates that the highest activity occurs at Pt_{2ML}/Os/C, where the corresponding OH binding is slightly (by ~0.03 eV) weaker than for Pt. This is a relatively rough approximation, but still a good way to find correlation between the theoretical prediction and experimental result.

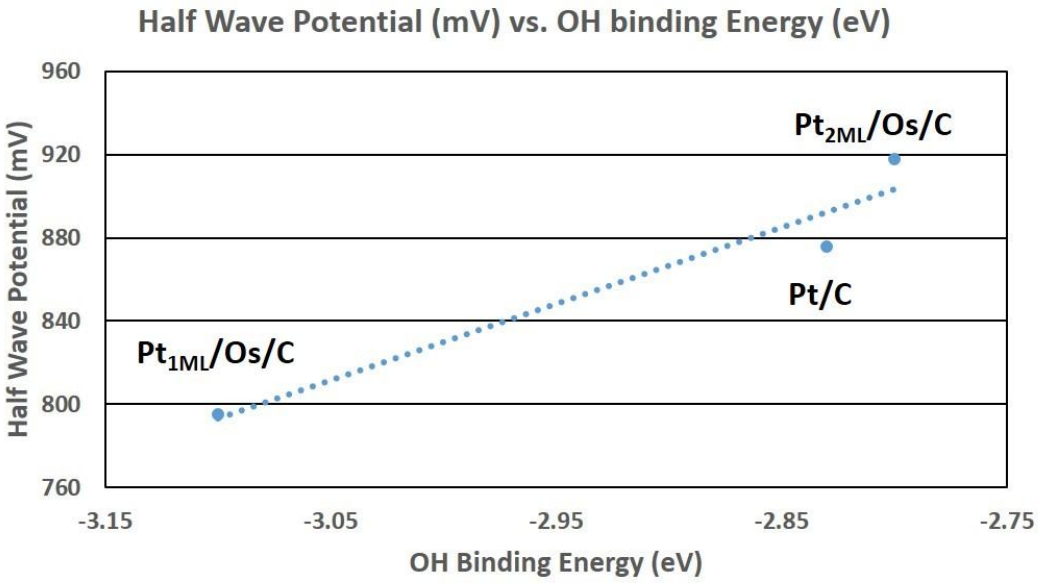

Figure S6. Experimental half wave potential vs. the theoretically predicted OH binding energy in solution.

In Figure S7, we use the calculated RDS for comparison with the experimental half wave potential. To fix the UPD coverage issue (Pt atoms partially cover the Os core), we used the average value of the RDS barriers for pure Os and Pt_{1ML}/Os (Table S5) as the RDS barrier for Pt_{1ML}/Os/C and the average value of the RDS barriers for Pt_{1ML}/Os and Pt_{2ML}/Os as the RDS barrier for Pt_{2ML}/Os/C. The higher barrier corresponds to the smaller half wave potential, and the correspondence looks good enough, although it is based on a rough approximation and assumption.

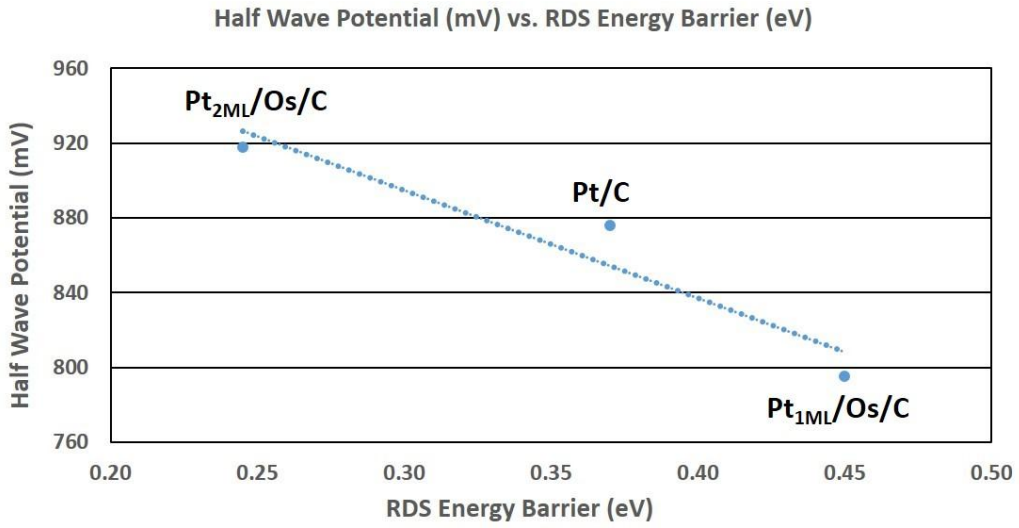

Figure S7. Experimental half wave potential versus the theoretical RDS reaction barrier in solution.

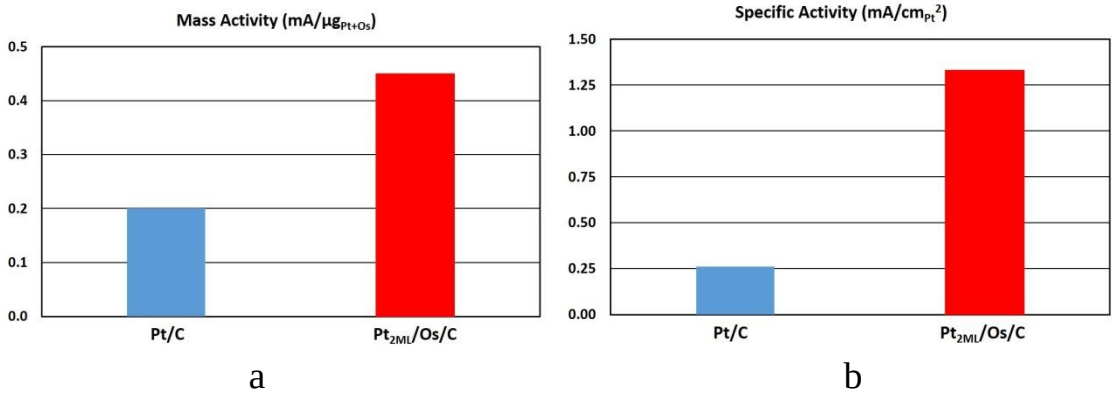

a b

Figure S8. The total precious mass (a) and specific (b) activity of Pt/C and Pt_{2ML}/Os/C at 0.9 V (vs. NHE).

Table S1. Calculated segregation energies (eV) for Pt_3M alloys with adsorbed O, adsorbed OH, and without adsorbates [bare (111) surfaces].[6] Positive energies indicate a favorable surface segregation. Only Pt_3Ir and Pt_3Os show good surface segregation in all three cases.

Alloy	O	OH	No adsorbate
Pt_3Ir	**0.12**	**0.27**	**0.57**
Pt_3Os	**0.09**	**0.51**	**1.33**
Pt_3Au	-0.01	-0.11	-0.33
Pt_3Rh	-0.14	0.05	0.39
Pt_3Ru	-0.15	0.25	0.83
Pt_3Pd	-0.17	-0.05	0.01
Pt_3Ag	-0.26	-0.18	-0.18
Pt_3Cu	-0.54	-0.07	0.14
Pt_3Co	-0.62	-0.05	0.50
Pt_3Ni	-0.62	-0.15	0.46
Pt_3Hg	-0.67	-0.60	-0.78
Pt_3Tc	-0.69	0.12	1.03
Pt_3Re	-0.87	0.44	1.69
Pt_3Cd	-0.91	-0.64	-0.47
Pt_3Zn	-0.95	-0.27	0.06
Pt_3Fe	-0.97	-0.44	0.02
Pt_3Mn	-1.61	-0.92	-0.12
Pt_3Cr	-1.92	-1.20	-0.02
Pt_3Mo	-1.92	-0.56	1.00
Pt_3W	-2.26	-0.72	1.37
Pt_3V	-2.45	-1.15	0.18
Pt_3Sc	-3.32	-2.75	-1.29
Pt_3Ti	-3.61	-2.69	-0.67
Pt_3Nb	-3.67	-2.39	-0.27
Pt_3Y	-3.93	-3.62	-2.45

Pt_3Ta	-4.29	-2.89	-0.28
Pt_3Zr	-4.31	-3.89	-2.06

All QM calculations were carried out using the SeqQuest software.[7] 4 layer 2x2 slabs were used for these calculations.

Table S2. Binding energies[a] (eV) of ORR species at various binding sites on Os, Pt and Pt/Os surfaces in gas phase.

Species	pure Os	pure Pt	Pt_{1ML}/Os	Pt_{2ML}/Os	Pt_{3ML}/Os
H/b	-2.72	-2.65	-2.34	-2.53	-2.69
H/f	**-2.80**	-2.66	-2.35	-2.53	-2.68
H/h	-2.71	-2.62	-2.34	-2.53	-2.66
H/t	-2.69	**-2.73**	**-2.45**	**-2.64**	**-2.81**
O/b	-4.57	-3.20	-2.90	-2.98	-3.16
O/f	-4.87	**-3.68**	**-3.16**	**-3.29**	**-3.55**
O/h	**-5.21**	-3.33	-2.97	-3.08	-3.27
O/t	-4.26	-2.62	-2.36	-2.29	-2.33
OH/b-f	**-3.24**	**-2.31**	-2.26	-2.17	-2.28
OH/b-h	-3.20	-2.30	-2.26	-2.17	-2.27
OH/f	Unstable[b]				
OH/h	Unstable[b]				
OH/t	-3.09	-2.28	**-2.27**	**-2.21**	**-2.29**
O_2/b	-1.80	**-0.56**	**-0.33**	**-0.28**	**-0.45**
O_2/f	-1.78	-0.49	-0.28	-0.19	-0.43

O_2/h	**-1.89**	-0.43	-0.30	-0.24	-0.44
OOH/t-b-f	unstable	-1.09	-1.02	-0.99	-1.11
OOH/t-b-h	unstable	**-1.09**	**-1.02**	**-0.99**	**-1.11**
OOH/t-f	**-1.73**	-1.01	-0.92	-0.91	-1.05
OOH/t-h	-1.68	-1.03	-0.91	-0.91	-1.05
HOOH/b	**-0.55**	**-0.27**	**-0.26**	**-0.29**	**-0.32**
HOH/t	**-0.50**	**-0.26**	**-0.23**	**-0.26**	**-0.30**
HOH-down/t	-0.05	-0.02	-0.05	-0.06	-0.09

[a] The estimated value for the basis set superposition error (BSSE) is ~0.05 eV.

[b]After geometry optimization, OH/f and OH/h moved to the bridge sites OH/b-f and OH/b-h.

Table S3. Binding energies[a] (eV) of ORR species at various binding sites on Os, Pt and Pt/Os surfaces in solution.

Species	pure Os	pure Pt	Pt_{1ML}/Os	Pt_{2ML}/Os	Pt_{3ML}/Os
H/b	-2.90	-2.76	-2.46	-2.63	-2.81
H/f	**-2.94**	-2.79	-2.46	-2.62	-2.78
H/h	-2.84	-2.75	-2.44	-2.61	-2.75
H/t	-2.83	**-2.82**	**-2.61**	**-2.72**	**-2.90**
O/b	-5.08	-3.95	-3.59	-3.65	-3.87
O/f	-5.26	**-4.49**	**-3.90**	**-4.11**	**-4.27**
O/h	**-5.67**	-4.05	-3.67	-3.82	-4.01
O/t	-5.17	-3.47	-3.59	-3.22	-3.19
OH/b-f	-3.50	-2.72	-2.79	-2.51	-2.62
OH/b-h	-3.38	-2.71	-2.70	-2.61	-2.65
OH/f	Unstable[b]				

OH/h	Unstable[b]				
OH/t	**-3.72**	**-2.83**	**-3.10**	**-2.80**	**-2.83**
O_2/b	**-2.56**	**-1.05**	**-0.86**	**-0.61**	**-0.87**
O_2/f	-2.21	-0.94	-0.78	-0.59	-0.85
O_2/h	-2.40	-0.83	-0.79	-0.57	-0.72
OOH/t-b-f	unstable	-1.55	**-1.73**	-1.45	-1.56
OOH/t-b-h	unstable	**-1.58**	-1.67	**-1.52**	**-1.58**
OOH/t-f	-2.24	-1.53	-1.52	-1.46	-1.49
OOH/t-h	**-2.35**	-1.50	-1.66	-1.39	-1.52
HOOH/b	**-0.84**	**-0.68**	**-0.58**	**-0.66**	**-0.71**
HOH/t	**-0.90**	**-0.67**	**-0.63**	**-0.65**	**-0.71**
HOH-down/t	-0.51	-0.46	-0.60	-0.50	-0.49

[a] The estimated value for the BSSE is ~0.05 eV.

[b] After geometry optimization, OH/f and OH/h moved to the bridge sites OH/b-f and OH/b-h.

Table S4. Reaction energy barriers (eV) for ORR steps on Os, Pt and Pt/Os surfaces in gas phase.

Step	Os	Pt	Pt_{1ML}/Os	Pt_{2ML}/Os	Pt_{3ML}/Os
HH dissociation	0.16	0.00	0.24	0.20	0.13
O_2 dissociation	0.00	0.56	0.90	0.77	0.63
OH formation	1.38	0.74	0.50	0.55	0.68
H_2O formation	**0.69**	0.26	**0.36**	0.23	0.19
OOH formation	0.81	**0.31**	0.18	0.23	**0.29**
OOH dissociation	0.00	0.09	0.29	0.27	0.17
H-OOH	0.00	0.06	0.29	**0.25**	0.23

dissociation					
O hydration	0.35	0.27	0.04	0.20	0.19

Table S5. Reaction energy barriers (eV) for ORR steps on Os, Pt and Pt/Os surfaces in solution.

Step	Os	Pt	Pt_{1ML}/Os	Pt_{2ML}/Os	Pt_{3ML}/Os
HH dissociation	0.14	0.00	0.15	0.15	0.09
O_2 dissociation	0.00	0.00	0.37	0.21	0.00
OH formation	1.92	1.09	0.61	0.83	0.92
H_2O formation	**0.64**	0.32	**0.26**	0.22	0.16
OOH formation	0.87	**0.37**	0.15	**0.23**	**0.35**
OOH dissociation	0.00	0.00	0.00	0.00	0.00
H-OOH dissociation	0.00	0.00	0.00	0.04	0.00
O hydration	0.42	0.45	0.06	0.37	0.42

Table S6. Binding energies[a] (eV) of ORR species on Pt, compressive Pt and Pt/Os surfaces in gas phase.

Species	Pt	compressive Pt	Pt_{1ML}/Os	Pt_{3ML}/Os
H	-2.73	-2.76	-2.45	-2.81
O	-3.68	-3.45	-3.16	-3.55
OH	-2.31	-2.23	-2.27	-2.29
O_2	-0.56	-0.33	-0.33	-0.45

OOH	-1.09	-1.02	-1.02	-1.11
HOOH	-0.27	-0.27	-0.26	-0.32
HOH	-0.26	-0.25	-0.23	-0.30

[a] The estimated value for the BSSE is ~0.05 eV.

Table S7. Binding energies[a] (eV) of ORR species on Pt, compressive Pt and Pt/Os surfaces in solution.

Species	Pt	compressive Pt	Pt_{1ML}/Os	Pt_{3ML}/Os
H	-2.82	-2.84	-2.61	-2.90
O	-4.49	-4.23	-3.90	-4.27
OH	-2.83	-2.79	-3.10	-2.83
O_2	-1.05	-0.77	-0.86	-0.87
OOH	-1.58	-1.53	-1.73	-1.58
HOOH	-0.68	-0.70	-0.58	-0.71
HOH	-0.67	-0.69	-0.63	-0.71

[a] The estimated value for the BSSE is ~0.05 eV.

Table S8. Reaction energy barriers (eV) for ORR steps on Pt, compressive Pt and Pt/Os surfaces in gas phase.

Step	Pt	Compressive Pt	Pt_{1ML}/Os	Pt_{3ML}/Os
HH dissociation	0.00	0.00	0.24	0.13
O_2 dissociation	0.56	0.63	0.90	0.63
OH formation	0.74	0.69	0.56	0.68
H_2O formation	0.26	0.22	**0.36**	0.19

OOH formation	**0.31**	**0.31**	0.18	**0.29**
OOH dissociation	0.09	0.14	0.29	0.17
H-OOH dissociation	0.06	0.24	0.29	0.23
O hydration	0.27	0.27	0.04	0.19

Table S9. Reaction energy barriers (eV) for ORR steps on Pt, compressive Pt and Pt/Os surfaces in solution.

Step	Pt	Compressive Pt	Pt_{1ML}/Os	Pt_{3ML}/Os
HH dissociation	0.00	0.00	0.15	0.09
O_2 dissociation	0.00	0.00	0.37	0.00
OH formation	1.09	0.92	0.61	0.92
H_2O formation	0.32	0.21	**0.26**	0.16
OOH formation	**0.37**	**0.37**	0.15	**0.35**
OOH dissociation	0.00	0.00	0.00	0.00
H-OOH dissociation	0.00	0.03	0.00	0.00
O hydration	0.45	0.47	0.06	0.42

REFERENCES

(1) Nørskov, J. K.; Rossmeisl, J.; Logadottir, A.; Lindqvist, L.; Kitchin, J. R.; Bligaard, T.; Jonsson, H. *J. Phys. Chem. B* **2004**, *108*, 17886-17892.

(2) Karlberg, G.; Rossmeisl, J.; Nørskov, J. K. *Phys. Chem. Chem. Phys.* **2007**, *9*, 5158-5161.

(3) Stephens, I. E. L.; Bondarenko, A. S.; Perez-Alonso, F. J.; Calle-Vallejo, F.; Bech, L.; Johansson, T. P.; Jepsen, A. K.; Frydendal, R.; Knudsen, B. P.; Rossmeisl, J.; Chorkendorff, I. *J. Am. Chem. Soc.* **2011**, *133*, 5485-5491.

(4) Rossmeisl, J.; Nørskov, J. K.; Taylor, C. D.; Janik, M. J.; Neurock, M. *J. Phys. Chem. B* **2006**, *110*, 21833-21839.

(5) Rossmeisl, J.; Karlberg, G. S.; Jaramillo, T.; Nørskov, J. K. *Faraday Discuss.* **2009**, *140*, 337-346.

(6) Tsai, H. C.; Yu, T. H.; Sha, Y.; Merinov, B. V.; Wu, P. W.; Chen, S. Y.; Goddard III, W. A. *J. Phys. Chem. C* **2014**, *118*, 26703-26712.

(7) Schultz, P. SeqQuest, Electronic Structure Code; Sandia National Laboratory, Albuquerque, NM: http://dft.sandia.gov/Quest/